SCIENCE RESULTS FROM SIXTEEN YEARS OF MRO SHARAD OPERATIONS. N. E. Putzig,[1,a] R. Seu,[2] G. A. Morgan,[1] I. B. Smith,[1] B. A. Campbell,[3] M. R. Perry,[1] and the MRO SHARAD Team, [1] Planetary Science Institute, Lakewood, CO, USA and Tucson, AZ, USA, [2] Sapienza Università di Roma, Roma, RM, Italia, [3] Smithsonian Institution, Washington, DC, USA, [a] Contact: nathaniel@putzig.com

Introduction: The Mars Reconnaissance Orbiter (MRO) began its primary science phase in October 2006. Over the ensuing 16 years of operations, the Shallow Radar (SHARAD) sounder acquired data along 32,000 discrete orbit segments ("observations") that cover 54% of the planet's surface at a 3-km cross-track resolution (Fresnel zone of the signal). We summarize the extensive science return from this rich dataset over this period, which informs both surface and subsurface properties of icy materials, volcanics, and sediments across Mars.

Polar Science: SHARAD has been especially effective in sounding of the Martian polar caps, whose cold temperatures and low lithic content often allow signals to penetrate through 2–3 km of icy layers, with enough dielectric contrast to provide reflections from up to 48 layer boundaries at depth [2,3].

Planum Boreum. In the north, the internal layering is illuminated relatively uniformly throughout the north polar layered deposits (NPLD), up to 2 km thick. Zones of high reflectivity alternate with zones of lower reflectivity [3,4], and low signal loss provides a strong argument for the purity of the ice (<~5% lithics) [5]. In Planum Boreum's main lobe, the NPLD sits atop a zone of diffuse reflectivity with no distinct basal return that corresponds to the basal cavi and rupēs units [6,7] whereas in much of the Gemina Lingula lobe, the NPLD appears to sit directly atop Vastitas Borealis units. A dramatic early finding is that the load of Planum Boreum materials has induced little to no lithostatic compensation, implying lower than expected heat flow and a thicker than expected lithosphere, at least in the north polar region [4]. While SHARAD's ~15-m vertical resolution hampers efforts to relate radar reflections to layering seen in visible imagery [8], intensive mapping efforts have revealed a host of internal features, including a buried chasma [9], trough-bounding surfaces extending through the upper ~1/2 of the NPLD [10], and a surface-conformal sequence at the top of the NPLD deposited after a latest Martian ice age [11,12]. An improved understanding of subsurface structures and the variability of dust content within the ice has been achieved through a combination of advanced processing techniques, such as 3D radar imaging [12,13] (**Fig. 1**), coherent and incoherent summation [12,14], and subband processing [15,16], and modeling of the radar response to different stratigraphies [17,18].

Planum Australe. In the south, the signal penetration depth and continuity of radar interfaces across the south polar layered deposits (SPLD) is much more variable than in the north [2,19,20]. At the pole in Australe Mensa, SHARAD revealed a near-surface deposit containing up to three layers of massive carbon dioxide ice with little to no internal radar reflectivity interspersed with thin layers of water ice [12,19,21]. The carbon dioxide ice contains sufficient mass to more than double atmospheric pressure if sublimated, which was likely the case prior to 350 ka [22]. Other zones of low reflectivity occur elsewhere in the SPLD, but they have not been shown to contain carbon dioxide ice, and areas of diffusive radar returns ("fog") permeate restricted zones or the entire stack of layers [19,20]. Surprisingly, the latter effect does not appear to be associated with a strong attenuation of the radar signal [23], in contrast to the similarly diffusive basal units of Planum Boreum.

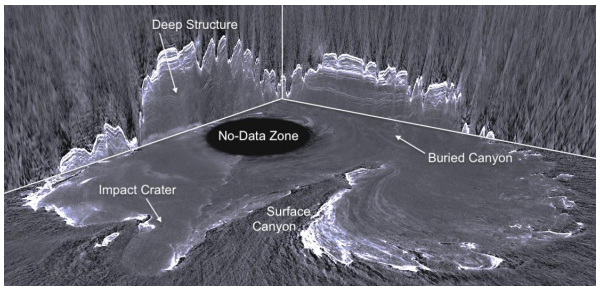

Figure 1. *Perspective view of the interior of Planum Boreum from 3D radar imaging [13], showing orthogonal vertical profiles through ≤ 2 km of NPLD and a horizontal slice across Gemina Lingula (right) and the main lobe. No-data zone is 300 km across (vertical exaggeration is 100:1).*

Non-polar Cryosphere: The periphery of many high-standing mesas in the mid-latitudes of Mars have long been known to contain apparent viscous-flow features, termed lobate debris aprons (LDAs), but their ice content was not well constrained prior to the arrival of SHARAD. Radar soundings of LDAs often obtain strong basal returns, demonstrating that the features are actually ice-rich debris-covered glaciers [24,25]. Surface roughness and interference from clutter signals often prevents or obfuscates the basal returns [26], but the latter effect can be addressed with 3D radar imaging, given sufficient coverage [27]. Beyond the LDAs, SHARAD also penetrates icy materials associated with pedestal craters [28] and obtains weaker reflections from what appears to be the base of ground ices in an isolated area around the Phoenix landing site [29] as well as in more extensive regions within Arcadia [30] and Utopia [31] Planitiae. While these mid-latitude ices are of high scientific interest

due to their connection to climate cycles on Mars, there have also been some efforts to better map their extent and nature with a view toward using the ice as a resource to sustain human missions, including enable fueling of Earth-return vehicles [32,33] (**Fig. 2**).

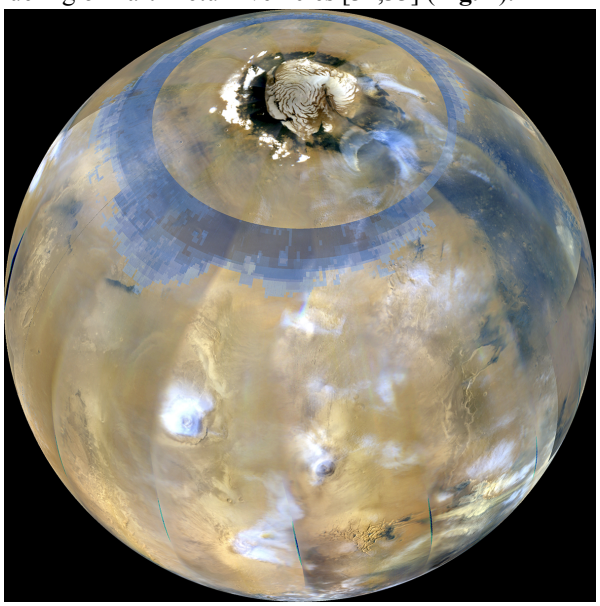

Figure 2. *Global view of Mars in a MRO Mars Color Imager mosaic overlain in blue shades with regions in the northern hemisphere of high consistency with the presence of near-surface ice in neutron and thermal spectrometer data, geomorphic feature mapping, and surface and subsurface radar analysis [31].*

Non-icy Terrains: The SHARAD signal also penetrates a range of other lithologies across Mars. Throughout Amazonian volcanic terrains, SHARAD reflections are observed from the base of lava flows, enabling recent eruption histories to be reconstructed (e.g. [15,34,35,36]). Dielectric and loss estimates derived from these detections also provide constraints on volcanic composition and density. In regions where lava has filled outflow channels, SHARAD detections offer a means to reconstruct channel morphology and measure the extent of prior fluvial erosion [37].

In select areas, SHARAD signals have penetrated sedimentary deposits, illuminating dielectric properties and associated stratigraphy. Together with other datasets, these results have informed depositional histories, such as the infilling of the ancient lowland surface of Amazonis [38] and the possible reworking of ash deposits surrounding Valles Marineris [39].

Ionosphere: In addition to subsurface sounding, SHARAD's measurements of the ionosphere's total electron content (TEC) provide a unique long-term record of the interaction of solar particles with Mars, including effects of the passage of comet Siding-Spring [40] and those of coronal-mass-ejection events [41]. Consistent spatial variations of the TEC also appear to be enabling new mapping of crustal magnetic fields [42].

Acknowledgments: The SHARAD Team is grateful to the MRO Project, the National Aeronautics and Space Administration (NASA), and Agenzia Spaziale Italiana (ASI) for ongoing support. ASI provided SHARAD to MRO and leads its operations through a contract to SHARAD Team Leader R. Seu at the Sapienza Università di Roma. SHARAD data are available at the Geosciences node of NASA's Planetary Data System via https://pds-geosciences.wustl.edu/missions/mro/sharad.htm.

References: [1] Seu R. et al. (2007) *JGR, 112*, E05S05. [2] Seu R. et al. (2007) *Science, 317,* 1715–1718. [3] Putzig N. et al. (2009) *Icarus, 204*, 443–457. [4] Phillips R. et al. (2008) *Science, 320,* 1182–1185. [5] Grima C. et al. (2009) *GRL, 36,* L03203. [6] Tanaka K. and Fortezzo C. (2012) *USGS Sci. Inv. Map 3177*. [7] Nerozzi S. and Holt J. (2018) *Icarus, 308,* 128–137. [8] Christian S. et al. (2013) *Icarus, 226,* 1241–1251. [9] Holt J. et al. (2010) *Nature, 465,* 446–449. [10] Smith I. and Holt J. (2010) *Nature, 465,* 450–453. [11] Smith I. et al. (2016), *Science, 352,* 1075–1078. [12] Putzig N. et al. (2022) *PSJ 3, 14 p*. [13] Putzig N. et al. (2018) *Icarus, 308,* 138–147. [14] Raguso C. et al. (2019) *5th IEEE Int. Workshop on Metrology for AeroSpace*. [15] Campbell B. and Morgan G. (2018) *GRL, 45,* 1759–1766. [16] Jawin E. et al. (2022) *GRL, 49,* 8 p. [17] Lalich D. et al. (2019), *JGR, 124,* 1690–1703. [18] Courville S. et al. (2021) *PSJ, 2,* 28 p. [19] Phillips R. et al. (2011) *Science, 332,* 838–841. [20] Whitten J. and Campbell B. (2018) *JGR, 123,* 1541-1554. [21] Alwarda R. and Smith I. (2021) *JGR, 126,* 5. [22] Bierson C. et al. (2016) *GRL, 43,* 4172–4179. [23] Abu Hashmeh et al. (2022) *JGR, 127,* 15 p. [24] Holt J. et al. (2008) *Science, 322,* 1235–1238. [25] Plaut J. et al. (2009) *GRL, 36,* L02203. [26] Petersen E. et al. (2018) *GRL, 45,* 11,595–11,604. [27] Perry M. et al. (2022) *19th Int. Conf. GPR*, abs. 110. [28] Nunes D. et al. (2011) *JGR, 116,* E04006. [29] Putzig N. et al. (2014) *JGR, 119,* 1936-1949. [30] Bramson A. et al. (2015) *GRL, 42,* 6566–6574. [31] Stuurman C. et al. (2016) *GRL, 43,* 9484–9491. [32] Morgan et al. (2021) *Nat. Astron., 5,* 230–236. [33] Putzig N. and Morgan G. et al. (in press), Ch. 16 in Badescu V. et al., eds., *Handbook of Space Resources, Springer Nature*. [34] Carter L. et al. (2009) *JGR 114,* E11. [35] Morgan G. et al. (2015) *GRL 42,* 7336-7342. [36] Ganesh I. et al. (2020) *J. Volcan. Geotherm. Res.* 390, 106748. [37] Morgan G. et al. (2013) *Science 340*, 607-610. [38] Campbell B. et al. (2009) *JGR 113,* E12010. [39] Mishev I. and Smith I. (2021) *LPSC LII,* Abs. 2548. [40] Restano M. et al. (2015) *GRL 42,* 4663-4669. [41] Lester M. et al. (2022) *JGR 127,* 22 p. [42] Campbell B. and Morgan G., this conference.